Polymer Chemistry

ROYAL SOCIETY OF CHEMISTRY

PAPER

View Article Online
View Journal | View Issue

Cite this: *Polym. Chem.*, 2026, **17**, 1706

Double metal cyanide (DMC) catalysis: detailed *in situ* NMR kinetics studies on the copolymerization of propylene oxide with substituted epoxides

Erik Kersten,†[a] Maximilian Kaiser,†[a,b] Jan Blankenburg,†[a,c] Kamil Maciol,[a] Manfred Wagner,[d] Sirus Zarbakhsh‡[e] and Holger Frey *[a]

Recently, the unusual copolymerization behavior of propylene oxide (PO) with ethylene oxide (EO) and glycidyl methyl ether (GME) using double metal cyanide (DMC) catalysis was demonstrated. Inspired by these results, the DMC-catalyzed copolymerization of PO with a large variety of alkyl and aryl epoxides, as well as other glycidyl ethers and -esters, was investigated by *in situ* ^{1}H NMR spectroscopy. This revealed a strong influence of the substituent of the epoxide monomer on the reactivity. With increasing steric demand of the alkyl or aryl group at the oxirane ring, the reactivity difference to PO increased drastically. Reactivity ratios for the copolymerization with PO for butylene oxide (BO) (r_{PO} = 4.7, r_{BO} = 0.21), 1,2-epoxyhexane (HexO) (r_{PO} = 16, r_{HexO} = 0.063), 3-methyl-1,2-epoxybutane (MEB) (r_{PO} = 29, r_{MEB} = 0.034) and styrene oxide (SO) (r_{PO} = 21, r_{SO} = 0.047) were determined. Due to the high steric demand of 3,3-dimethyl-1,2-epoxybutane (DMEB) in the copolymerization experiment with PO, only homopolymerization of PO was observed. Additionally, the copolymerization behavior of PO with various glycidyl ethers (GE) was investigated. This revealed similar reactivity ratios for all glycidyl ethers in a range of r_{PO} = 9.2–21 and r_{GE} = 0.11–0.048. Further investigation of the two glycidyl esters, glycidyl methacrylate (GMA) (r_{PO} = 20, r_{GMA} = 0.050) and glycidyl benzoate (GBz) (r_{PO} = 33, r_{GBz} = 0.031), was conducted as well. The extensive studies give insight into the compatibility of different comonomers in DMC catalysis and confirm its high substrate selectivity, specifically for the PO monomer. The influence of steric demand and electronic structure of individual monomers was assessed using $\%V_{Bur}$, Hirshfeld partial charges, and ΔN (electron transfer to Zn^{2+}) and discussed in the context of comonomer reactivity relative to PO under DMC catalysis.

Received 4th February 2026,
Accepted 26th March 2026

DOI: 10.1039/d6py00118a

rsc.li/polymers

Introduction

Poly(propylene oxide) (PPO) is most often industrially prepared by base-catalyzed anionic ring-opening polymerization (AROP).[1] However, the well-known drawbacks of AROP include chain transfer reactions of propylene oxide (PO), leading to allyl end groups, broadened molecular weight distributions, and reduced hydroxyl end-group functionality,[2] while residual alkali metal salts present in the final polymer must further be removed for many subsequent applications.[3]

To overcome these limitations, heterogeneous double metal cyanide (DMC) catalysts were developed by General Tire and Rubber Company in 1963 and are now well established for the commercial production of PPO-based polyether polyols.[3–6] Compared with conventional AROP, DMC catalysis exhibits very low levels of side reactions,[7] resulting in narrow molecular weight distributions of the respective PPO.[8,9] Furthermore, catalyst loadings as low as 25 ppm are sufficient for PO polymerization, allowing omission of catalyst removal after synthesis and direct use of the resulting PPO polyol for subsequent applications.[3,10]

A typical characteristic of DMC-catalyzed PO polymerization is the presence of an induction period, which is generally attributed to catalyst activation and has been investigated experimentally and computationally.[3,4,11] More recently, Kim *et al.* introduced a new type of DMC catalyst modified with organic carbonates as complexing agents (CA).[12] The experi-

[a]*Department of Chemistry, Johannes Gutenberg University, Duesbergweg 10-14, 55128 Mainz, Germany. E-mail: hfrey@uni-mainz.de*
[b]*Max Planck Graduate Center, Forum Universitatis 2, 55122 Mainz, Germany*
[c]*Graduate School Materials Science in Mainz, Staudinger Weg 9, 55128 Mainz, Germany*
[d]*Max Planck Institute for Polymer Research, Ackermannweg 10, 55128 Mainz, Germany*
[e]*BASF SE, Carl-Bosch-Straße 38, 67056 Ludwigshafen am Rhein, Germany*
†These authors contributed equally to this work.
‡Deceased.

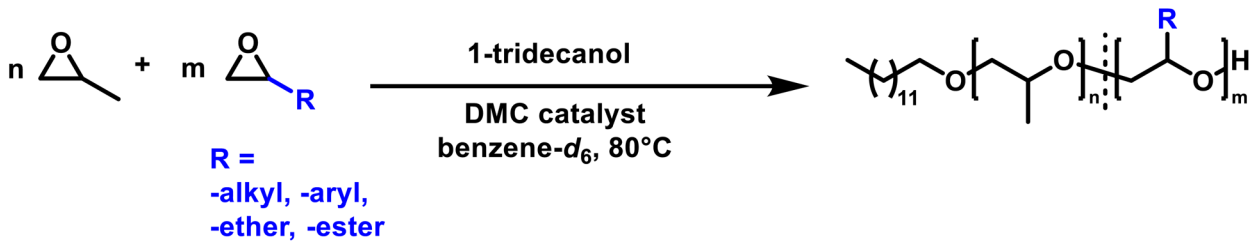

Scheme 1 Copolymerization experiments of PO with various epoxide derivatives under DMC catalysis using 1-tridecanol as an initiator. Structures of all epoxide monomers are shown in Table 1.

mental induction time data were further interpreted by density functional theory (DFT) calculations and crystal structural analysis, identifying the fraction of ligand-driven electron transfer (ΔN) as a descriptor for catalyst–substrate coordination relevant to activation of the DMC catalyst.[3]

DMC catalysis also exhibits unusual kinetic behavior, including the so-called "catch-up kinetics", which has been associated with narrow molar-mass distributions and may also be linked to the commonly observed high-molecular-weight tailing (HMWT) in DMC-catalyzed polymerizations.[5,13–15] The active sites of DMC catalysts are assumed to have a cationic coordinative character, but the precise mechanism remains difficult to verify unambiguously due to the complexity of the heterogeneous catalyst system and the crucial interplay of micro- and macrokinetic factors, including surface chemistry and diffusion-dependent processes.[8,16–18] Furthermore, the method of preparation and choice of complexing agents (CA) can significantly influence the DMC catalyst activity, further rendering comparative studies highly challenging.[19,20] Despite its industrial relevance, DMC catalysis has received comparatively limited academic attention, possibly because the elevated polymerization temperatures and pressures typically necessitate the use of an autoclave-based reaction setup.

Atactic PPO is an amorphous and hydrophobic polymer with a low glass-transition temperature of −73 °C,[21] making it attractive for the synthesis of non-ionic surfactants and application in flexible PU foams or lubricants.[22] While copolymerization of PO with butylene oxide (BO) or styrene oxide (SO) enables further tuning of the thermal and physicochemical behavior of the resulting polyol copolymers,[23] incorporation of functional epoxides such as glycidyl ethers introduces additional functionality into the otherwise inert PPO backbone.[19,24]

In the last decade, several works have demonstrated the compatibility of DMC catalysts with different alkylene oxide derivatives and even functional epoxides like glycidol, epichlorohydrin or glycidyl methacrylate.[25,26] However, most of these studies focus on either the homopolymerization of the epoxide derivatives or copolymerization with carbon dioxide or cyclic anhydrides.[27] Surprisingly, the copolymerization of the said epoxides with PO, which is by far the most commonly employed substrate for DMC catalysis, is very rarely investigated in detail.[3,18] Recently, our group reported the unusual copolymerization behavior of the comonomer pair PO and EO (r_{PO} = 2.4 and r_{EO} = 0.42) under DMC catalysis, which revealed an inverse reactivity compared to other polymerization conditions.[28] Moreover, a subsequent study by Matthes *et al.* revealed the unexpectedly high reactivity ratios for the hydrophilic glycidyl methyl ether (GME) in the DMC-catalyzed copolymerization with PO, resulting in near-ideal random copolymers (r_{PO} = 1.40 and r_{GME} = 0.71) with tunable thermoresponsiveness.[29] These studies already indicate that the DMC catalyst demonstrates an unexplored and unique substrate specificity toward different epoxide comonomers, which does not follow the trends observed in other common living polymerization techniques such as conventional AROP or MAROP.[30] Intrigued by these findings, we further investigated the DMC-catalyzed copolymerization of PO with a variety of alkyl oxides (AlkO), aryl epoxides (ArO), glycidyl ethers (GE) and glycidyl esters (GEs) to elucidate substrate-specific reactivity trends, which are key determinants of the resulting copolymer structure in the copolymerization of PO with other epoxides under DMC catalysis (Scheme 1 and Table 1).

In situ ^{1}H NMR kinetics proved to be a powerful tool to monitor the copolymerization kinetics of PO with other epoxides under DMC catalysis, which could be well described with the ideal copolymerization model.[31–33] Copolymerization kinetics and monomer reactivities towards the DMC catalyst are specifically investigated from the perspective of the epoxide substrate. We further support and interpret the experimental kinetic data, using complementary DFT computations, to unveil substrate limitations of the catalyst, as well as the influence of monomer geometry and electronic structure on its corresponding reactivity in the copolymerization reaction.

Experimental

A detailed description of all synthesis procedures, reagents and instrumentation, as well as performed computations *via* density functional theory (DFT), is provided in the SI.

Results and discussion

Systematic investigation of the copolymerization of PO with alkyl and aryl epoxides

Recently, the copolymerization of PO and EO under DMC catalysis surprisingly revealed the higher reactivity of PO under

Table 1 Overview of epoxide monomer structures (with residual R in blue) investigated in the DMC-catalyzed *in situ* copolymerization kinetic experiments. Monomers are ordered by the respective epoxide substance classes: alkylene oxide (AlkO), aryl epoxide (ArO), glycidyl ether (GE) and glycidyl ester (GEs)

Epoxide class	Comonomer structure with residual (R)
Alkylene oxide (AlkO)	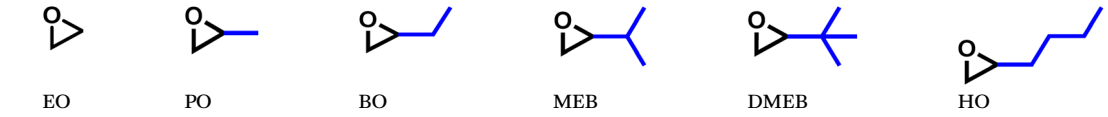 EO PO BO MEB DMEB HO
Aryl epoxide (ArO)	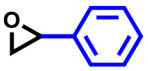 SO
Glycidyl ether (GE)	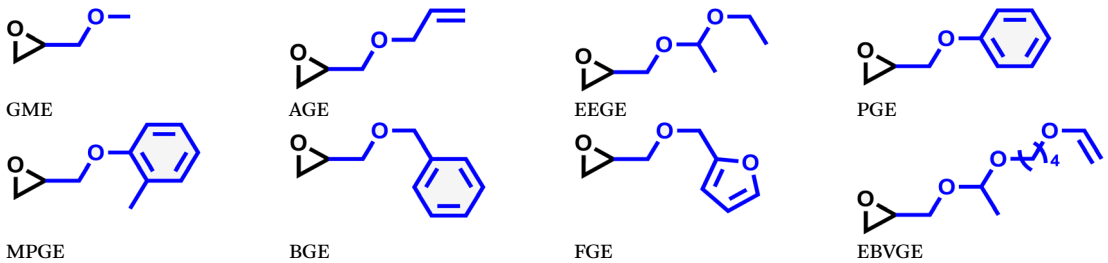 GME AGE EEGE PGE MPGE BGE FGE EBVGE
Glycidyl ester (GEs)	 GMA GBz

these conditions.[28] The reactivity ratios are in contrast to the steric demand of this comonomer pair and seem to be dominated by electronic effects. A possible explanation for the selectivity for PO is the higher basicity of the monomer due to the +I effect of the additional methyl group compared to EO. This could lead to better coordination of the oxygen to the active sites of the DMC catalyst. To further investigate the copolymerization behavior of PO under DMC catalysis, various alkylene oxides and glycidyl ether comonomers were investigated *via in situ* ^{1}H NMR kinetic experiments in this work. Table S1 (SI) provides an overview of all experimentally determined molar ratios of PO to the comonomer ($n_{PO}:m_{Co}$) for the copolymerization kinetics experiments performed in this work. These ratios were determined from the first recorded ^{1}H NMR spectrum, acquired prior to the start of the copolymerization. In addition, Table S1 summarizes the theoretically expected molecular weights ($M_n^{Theo.}$) of the respective copolymers formed during the *in situ* ^{1}H NMR kinetic experiments.

A systematic approach was used to investigate the influence of the steric demand of the epoxy alkyl chain. Although DMC catalysis is most commonly conducted in bulk, we employed benzene-d_6 (33 wt%) as a cosolvent to reduce viscosity and diffusion-dependent microkinetic effects during the copolymerization, as we were predominantly intrigued by the primary influence of monomer structure on its reactivity towards the catalyst. PO was initially copolymerized with the nearest analogues in the alkyl epoxide series: butylene oxide (BO). To study the copolymerization behavior of PO and BO, an *in situ* ^{1}H NMR kinetics experiment in benzene-d_6 was performed at 80 °C. The consumption of both monomers could be followed by the disappearance of the epoxide protons, as shown in Fig. 1.

As evidenced in Fig. 1 and 2, in the copolymerization of PO and BO, an induction period (t_i) of 18 min could be observed (Table 2). During this initial period, almost no conversion of the monomers was detected. At the end of the induction period, a strong increase in polymerization rate can be noticed, which leads to full conversion of both monomers within 30 min. From these data, the comonomer concentration as a function of time or total conversion can be extracted (Fig. 2). MALDI-ToF mass spectrometry was performed to ensure the formation of well-defined copolymers (SI, Fig. S2). The mass spectra revealed copolymer chains exclusively initiated by 1-tridecanol, while all peaks could further be assigned to a linear combination of the two comonomers.[34] This verifies the formation of copolymers, while a polymer blend of both homopolymers can be excluded. In the following experiments, for the determination of the reactivity ratio (r) and half-life ($t_{1/2}$), only the time interval after the end of the induction period (t_i) until complete consumption of PO is considered. It is evident that PO was consumed at a much faster rate compared to BO.

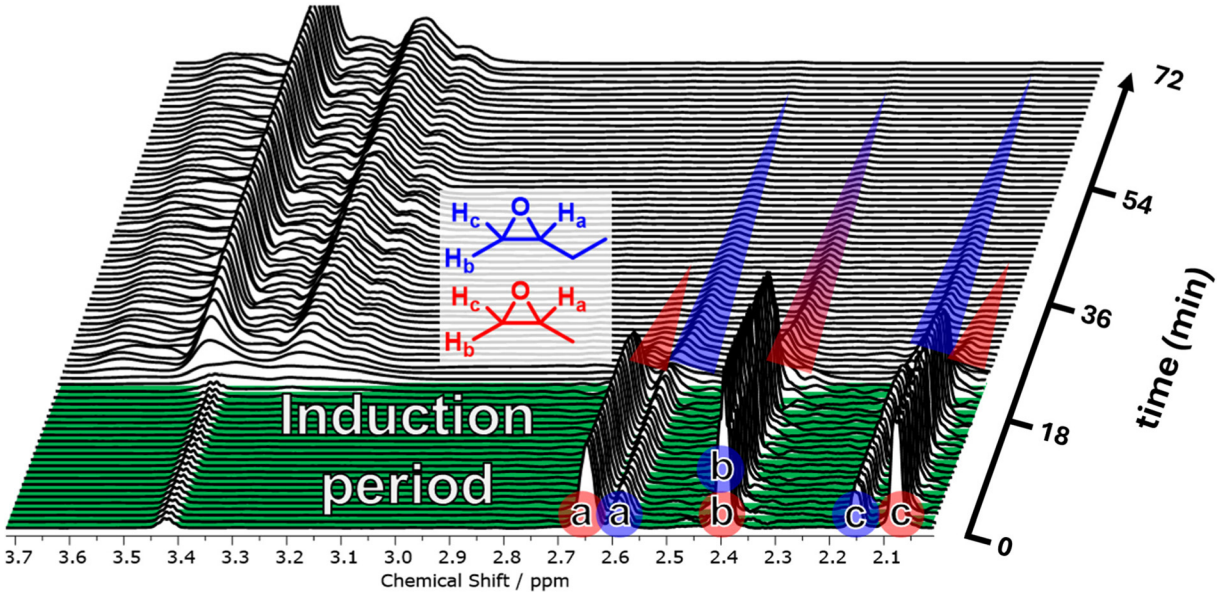

Fig. 1 ^{1}H NMR spectra (500 MHz, benzene-d_6) of the copolymerization of PO and BO using DMC catalysis with the highlighted induction period.

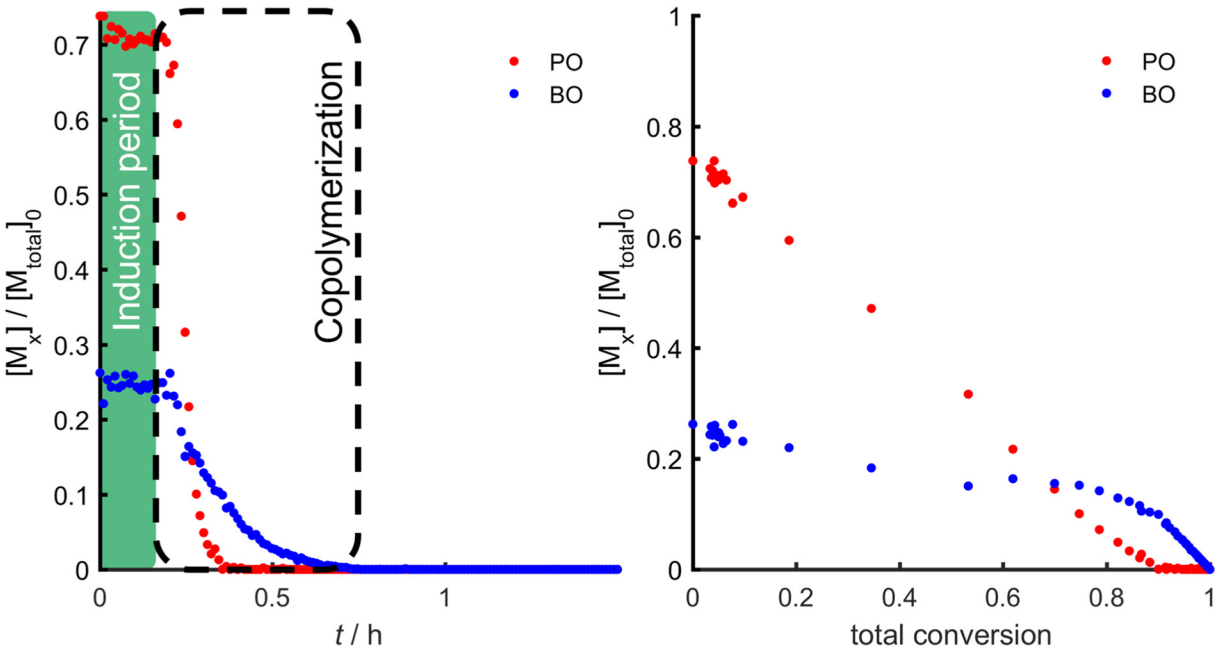

Fig. 2 Data of the copolymerization experiment of PO (red) and BO (blue). Left: individual monomer concentrations $[M_x]$ normalized by the total monomer concentration $[M_{total}]_0$ as a function of time t with time intervals for the induction period (green) and copolymerization (dashed frame). Right: individual monomer concentrations $[M_x]$ normalized by the total monomer concentration $[M_{total}]_0$ plotted *vs.* total conversion of both monomers for the time interval of copolymerization after the induction period.

The reactivity ratios were determined by fits of the non-terminal integrated ideal model, which was introduced in a recent work.[28] All fits were performed with weights proportional to the total monomer concentration. The corresponding Jaacks fit and the fit of the integrated ideal model can be found in Fig. S2 (SI).[32] The obtained reactivity ratios for the copolymerization of PO and BO obtained by the integrated ideal fit were r_{PO} = 4.7 and r_{BO} = 0.21. In all cases, the Jaacks fits gave very similar values, which are summarized in Tables S1 and S2 (SI). The corresponding SEC trace of the P(PO-*co*-BO) copolymer reflects a narrow monomodal distribution with a low dispersity of $Đ$ = 1.13 (Fig. 3). This clearly demonstrates

Table 2 Reactivity ratios, induction times and half-lives determined for the copolymerization of PO with alkylene oxide (AlkO) and aryl epoxide (ArO) comonomers *via* the integrated ideal model

Comonomer	Structure	r_{PO}	r_{Co}	t_i/min	$t_{1/2}$ (PO)/min	$t_{1/2}$ (Co)/min	ΔN
PO-d_6 [a]	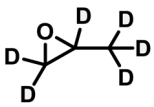	1.0	1.0	—	32	32	0.077
EO[28]		2.4	0.42	<1.5	2.6	5.3	0.078
BO	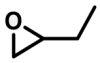	4.7	0.21	18	1.3	7.5	0.075
HexO	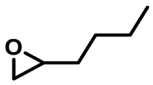	16	0.063	37	3.3	48	0.071
SO	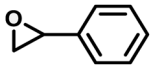	21	0.047	26	3.3	53	0.051
MEB		29	0.034	39	2.0	84	0.071
DMEB[b]	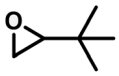	≫1	≈0	40	4.1	—	0.069

[a] No induction period could be observed; reactivity ratios determined *via* the Jaacks fit. [b] Only homopolymerization of PO was observed.

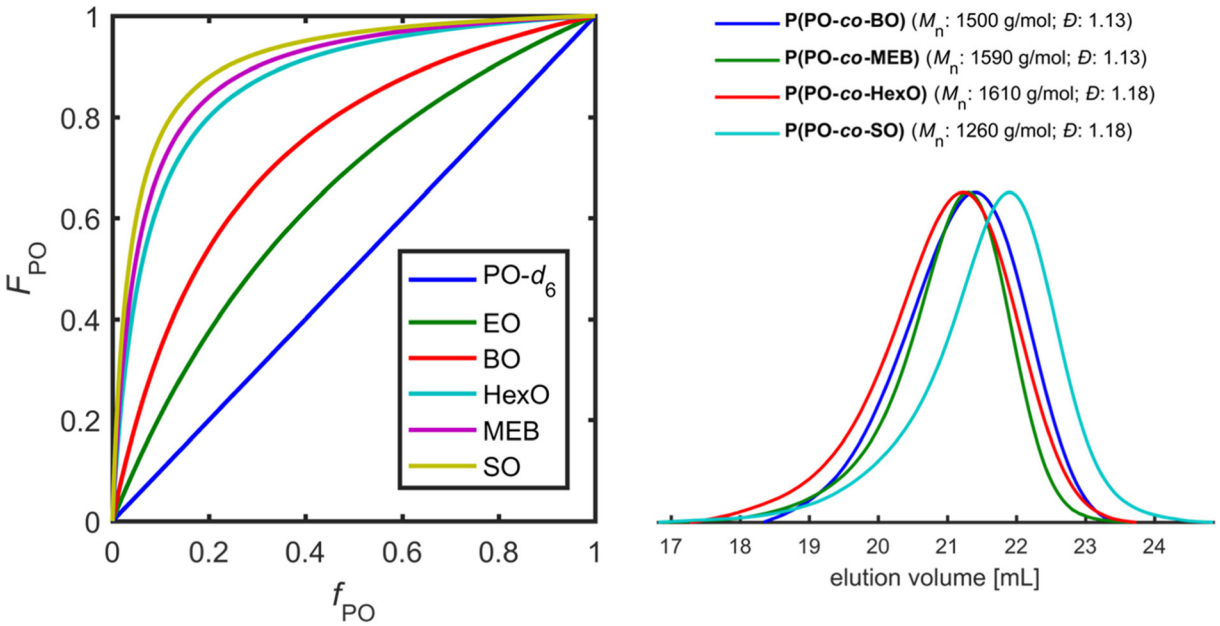

Fig. 3 Left: copolymerization diagram for DMC-catalyzed copolymerizations of PO with epoxide comonomers. Right: SEC traces (DMF, PEG calibration) of the corresponding copolymers.

the controlled character of the DMC-catalyzed copolymerization, even in the absence of stirring or homogeneous mixing in the NMR tube during the kinetic experiment.

Another feature of a controlled polymerization is the pseudo-first-order kinetics behavior, which indicates that the number of active chains is constant during the polymerization.[35] This results in a linear behavior of the logarithmic concentration $\ln([M]_0/[M])$ over time. The slope of the individual plots corresponds to the apparent rate constant for the exponential consumption of each monomer. From these rate constants, the half-lives ($t_{1/2}$) for each monomer were calculated (Table 2).

Furthermore, the fraction of the rate constants is directly equal to the reactivity ratio in the ideal case.[31] The reactivity ratios determined by the fraction of the apparent rate constants are given in Tables S2 and S3 (SI). The narrow molecular

weight distribution and the pseudo-first-order kinetic behavior imply an initiation of all chains after the induction period at the start of the copolymerization.

Consequently, owing to the different reactivities of the comonomers, a compositional gradient along the copolymer chains is expected, with preferential incorporation of PO at the start of the chain and a higher likelihood of incorporation of the AlkO or ArO comonomer towards the chain end. However, we must emphasize that direct translation of reactivity ratios into a microstructure that reflects the compositional comonomer profile along individual growing chains is valid only for ideally living polymerizations.[36] In this context, DMC catalysis is better described as quasi-living and governed by diffusion-dependent "catch-up kinetics", where individual polymer chains reversibly activate and deactivate through molecular-weight-dependent association and dissociation at catalytic sites, which modulates the homogeneous chain growth.[14] Although the average molecular weight of the batch can increase linearly with the total monomer conversion,[37] this does not necessarily hold true for individual chains, which is where DMC catalysis diverges from ideally living systems such as AROP. For this reason, we refrain from directly proposing a precise microstructure solely based on reactivity ratios derived from the monomer conversion data. Nonetheless, the presented values provide a reasonable first-order estimate of the expected compositional trends averaged over the whole polymer batch.

To test whether the monomer's electronic structure influences reactivity, we calculated DFT Hirshfeld charges for the epoxide ring atoms (SI, Scheme S3; Tables S4 and S4), which showed no significant differences between individual AlkO/ArO monomers. Pearson-type fractions of electron transfer to the Zn^{2+} site ($\Delta N > 0$), computed from HOMO/LUMO descriptors, likewise showed little variation across the monomer series (ΔN = 0.078 to 0.069; Table S7). Following a concept recently described by Kim *et al.*, no higher coordination tendency of any AlkO/ArO monomer toward the DMC surface is therefore to be expected.[12] Only SO exhibits a distinctly lower ΔN value (0.051), consistent with its conjugated aromatic system and the reduced HOMO/LUMO gap. Consequently, the reactivity of AlkO and ArO is governed primarily by the geometry and steric demand of the substituent adjacent to the epoxide ring.

To further test this conjecture, we systematically increased the steric demand of the AlkO/ArO comonomer. Relative to BO, 3-methyl-1,2-epoxybutane (MEB) carries an additional methyl group in the α-position next to the epoxide ring and accordingly shows a larger discrepancy in reactivity ratios compared to the PO/BO pair (SI, Fig. S3; r_{PO} = 29 and r_{MEB} = 0.034). These results highlight the strong influence of the pendant group on the comonomer reactivity. Adding a second α-methyl group leads to the monomer 3,3-dimethyl-1,2-epoxybutane (DMEB), which appears to exceed the steric tolerance of the DMC catalyst used in this study. Accordingly, only PO homopolymerization was observed, while the DMEB concentration remained unchanged throughout the copolymerization experiment (SI, Fig. S4). This indicates that DMEB is essentially unreactive toward the DMC catalyst under our PO copolymerization conditions.

With this knowledge regarding the steric limitations of the DMC catalyst, copolymerization of PO with HexO (1,2-epoxyhexane), a constitutional isomer of DMEB, was further studied (SI, Fig. S5). By reducing the steric demand of the substituted α-carbon next to the epoxide ring, the reactivity ratio of the comonomer (r_{PO} = 16 and r_{HexO} = 0.063) increased compared to MEB and DMEB. This shows a reactivity difference between BO and MEB and is in line with the steric demand of the linear alkyl side chain of HexO compared to the bulky, branched isopropyl- and isobutyl groups of MEB and DMEB. Further increasing the size of the substituent to a phenyl group with the comonomer styrene oxide (SO) revealed reactivity ratios of r_{PO} = 21 and r_{SO} = 0.047 (SI, Fig. S6). These reactivity ratios are very close to the monomer pair PO/MEB and are consistent with the similar steric demand of MEB and SO.

The exceptionally high substrate specificity of the DMC catalyst toward PO prompted us to examine whether even the smallest possible modification of the PO substrate affects its reactivity in DMC-catalyzed copolymerization. For this purpose, deuterated propylene oxide (PO-d_6) was selected as the closest possible analogue of PO, preserving the molecular structure while differing only by isotopic substitution. In this way, potential effects of isotopic substitution on monomer reactivity could be probed without introducing additional steric or electronic changes associated with a different comonomer structure. The *in situ* kinetic study was performed analogously to the preceding copolymerization experiments. In this experiment, two simultaneous NMR kinetic experiments were performed: the first channel recorded the ^{1}H nuclei, while a second channel scanned the ^{2}H nuclei. The ^{1}H spectra show only the consumption of the monomer PO. In the ^{2}H experiment, the conversion of PO-d_6 is visible (SI, Fig. S7). The integrated ideal equation could not provide a good fit, as it is fundamentally not defined for the composition-invariant case with reactivity ratios $r_1 = r_2 = 1$. In this drift-free case ($f_{PO} = F_{PO}$), the reactivity ratios could only be determined by the linear Jaacks fit. The respective fit revealed no differences in the reactivities of PO and deuterated PO-d_6, corresponding to a perfectly random copolymerization, further demonstrating no effect of isotopic substitution on monomer reactivity in DMC catalysis.

The results of the copolymerization experiments of PO with AlkO and ArO are summarized in Table 2. The SEC traces and copolymerization diagrams of the copolymers consisting of PO and AlkO or ArO are shown in Fig. 3. Despite the lack of stirring in the NMR tube, the copolymerization under heterogeneous DMC catalysis led to well-defined copolymers with low dispersities ($Đ$ < 1.2) for all copolymers formed in the NMR tube. The molecular weights determined by SEC for all copolymers were in good agreement with the theoretically expected M_n values, which were calculated from the molar ratio of PO to the comonomer in the first recorded ^{1}H NMR spectrum for each kinetic copolymerization experiment (SI,

Table S1). Minor deviations in M_n can be attributed to a slight underestimation by SEC, due to the differing hydrodynamic radii of the investigated copolymers compared with the employed PEG calibration standard.

The half-life of PO throughout all experiments was relatively unaffected by the type of comonomer and was typically in a range of 1–4 min. This demonstrates the high tolerance of the DMC catalyst toward different comonomers, although a general increase in induction time (t_i) with increasing comonomer steric demand was observed. This might result from the sterically hindered coordination of the monomers to the active Zn site, which is an essential step in the activation of the DMC catalyst.

To further quantify this trend, we calculated the percentage of buried volume $\%V_{Bur}$ of the coordinating epoxide oxygen O^1 for each monomer using the web tool SambVca 2.1.[38] Although $\%V_{Bur}$ is frequently employed as a steric index for analysis of catalyst pockets, it can further be used to describe the steric accessibility of coordinating epoxide substrates to a metal centre as well.[39,40] As the structure of the heterogeneous DMC catalyst can significantly vary depending on the preparation method, and further undergoes drastic changes due to fragmentation processes during catalysis, we primarily investigated $\%V_{Bur}$ from the perspective of the epoxide substrates.[41] All $\%V_{Bur}$ values for the oxygen O^1 and unsubstituted methylene group C^1 in the epoxide ring of the monomers are summarized in Tables S9 and S10 (SI) and are calculated for a sphere around the designated atom with a radius of 3.5 Å. Here, higher values correspond to higher steric hindrance of the respective atom. As expected, the unreactive monomer DMEB showed the highest $\%V_{Bur}$ for O^1 and C^1. By comparing the topographic steric maps of PO and DMEB, it becomes evident that the highly bulky *tert*-butyl group of DMEB shields both O^1 and C^1, potentially inhibiting the coordination to the active Zn site of the catalyst, as well as the nucleophilic attack on C^1, which is essential for the subsequent ring-opening and propagation reaction (Fig. 4). While DMEB cannot reduce the steric demand of the side chain *via* conformational change, as HexO can, additional steric repulsion from co-ligands or coordinating polymer chains at the active Zn site may completely inhibit the DMEB polymerization (SI, Scheme S2).

By plotting the determined reactivity ratios r_{AE} of the monomers *vs.* the respective $\%V_{Bur}(C^1)$, a clear trend becomes evident in which monomer reactivity decreases with increasing steric shielding at C^1 (Fig. 5). Additionally, a general increase in induction time (t_i) with increasing steric hindrance at O^1 in the respective comonomer was observed. However, induction times in DMC-catalyzed copolymerizations can fluctuate significantly, which may explain the slight deviations of HexO and MEB from this trend.[42]

Here, PO-d_6, which is representative of regular PO, completely deviates from both trends, since no induction period was observed and the monomer exhibited the highest reactivity ratio. From this, we conclude that even small deviations from the ideal PO molecular geometry result in strong changes in AlkO or ArO monomer reactivity.

Copolymerization of PO with glycidyl ethers

In a previous work, our group reported the copolymerization of PO with glycidyl methyl ether (GME) in bulk *via* DMC catalysis. Although GME is sterically slightly more demanding than EO or BO, the study revealed high reactivity ratios for GME (r_{GME} = 0.71 and r_{PO} = 1.40), yielding nearly ideal copolymers with PO.[29] Further motivated by the astonishing results for the copolymerization of PO with alkyl and aryl epoxides, we also investigated the copolymerization kinetics of PO with various glycidyl ethers, as shown in Table 3.

Similar to the kinetic study in the previous section, we systematically increased the steric demand of the GE comonomers. In this regard, AGE is one of the most frequently employed epoxides for introducing functional groups into polyethers.[43] Copolymerization of PO with AGE revealed clear deviation from the near ideally random copolymerization of the PO/GME pair. Reactivity ratios (Fig. 6; r_{PO} = 9.2 and r_{AGE} = 0.11) further suggest the formation of a gradient copolymer.

Another important glycidyl ether is furfuryl glycidyl ether (FGE), which enables polyether modification *via* the Diels–Alder reaction and has been applied in self-healing materials based on poly(ethylene oxide)-*block*-poly(furfuryl glycidyl ether) (PEG-*b*-PFGE) block copolymers.[44] The copolymerization results are shown in Fig. S9 (SI) and gave reactivity ratios of r_{PO} = 14 and r_{FGE} = 0.073. The next comonomers investigated were benzyl glycidyl ether (BGE) (SI, Fig. S10; r_{PO} = 12 and r_{BGE} = 0.081) and phenyl glycidyl ether (PGE) (SI, Fig. S11; r_{PO} = 14 and r_{PGE} = 0.073), for which no major discrepancies in comonomer reactivity could be observed. Further increasing the steric demand, copolymerization of the related *o*-methylphenyl glycidyl ether (MPGE) showed reactivity ratios of r_{PO} = 17 and r_{MPGE} = 0.064 (SI, Fig. S12). From the reactivity ratios, induction and half-lives summarized in Table 3, no clear correlation between substituent steric demand and the observed reaction behavior can be established. Apart from GME and AGE, all examined glycidyl ethers demonstrated very similar reactivity, indicating the potential formation of strong gradient or tapered block copolymer structures, as implied by the copolymerization diagrams (Fig. 7).

The computed $\%V_{Bur}(O^1)$ and $\%V_{Bur}(C^1)$ values were also in a similar range of 40 (C^1) to 46 (O^1) for all glycidyl ethers (SI, Table S10), which further demonstrates the limitation of this steric descriptor. The flexible ether side chain allows glycidyl ethers to moderate the steric bulk through change of conformation. While $\%V_{Bur}$ is reliable for free molecules with constrained geometries, such as the presented AlkO or ArO monomers, the values become less precise and can change drastically depending on the molecular conformation.[39] As no clear trend in induction times could be observed, the monomer reactivity behavior of glycidyl ethers is more complex and cannot be exclusively described by steric factors.

Even though DFT calculations revealed no major change in the charge distribution of the epoxide-ring atoms for all glycidyl ethers (Table S5), the calculated fraction of electron transfer (ΔN) shows larger differences among individual GE mono-

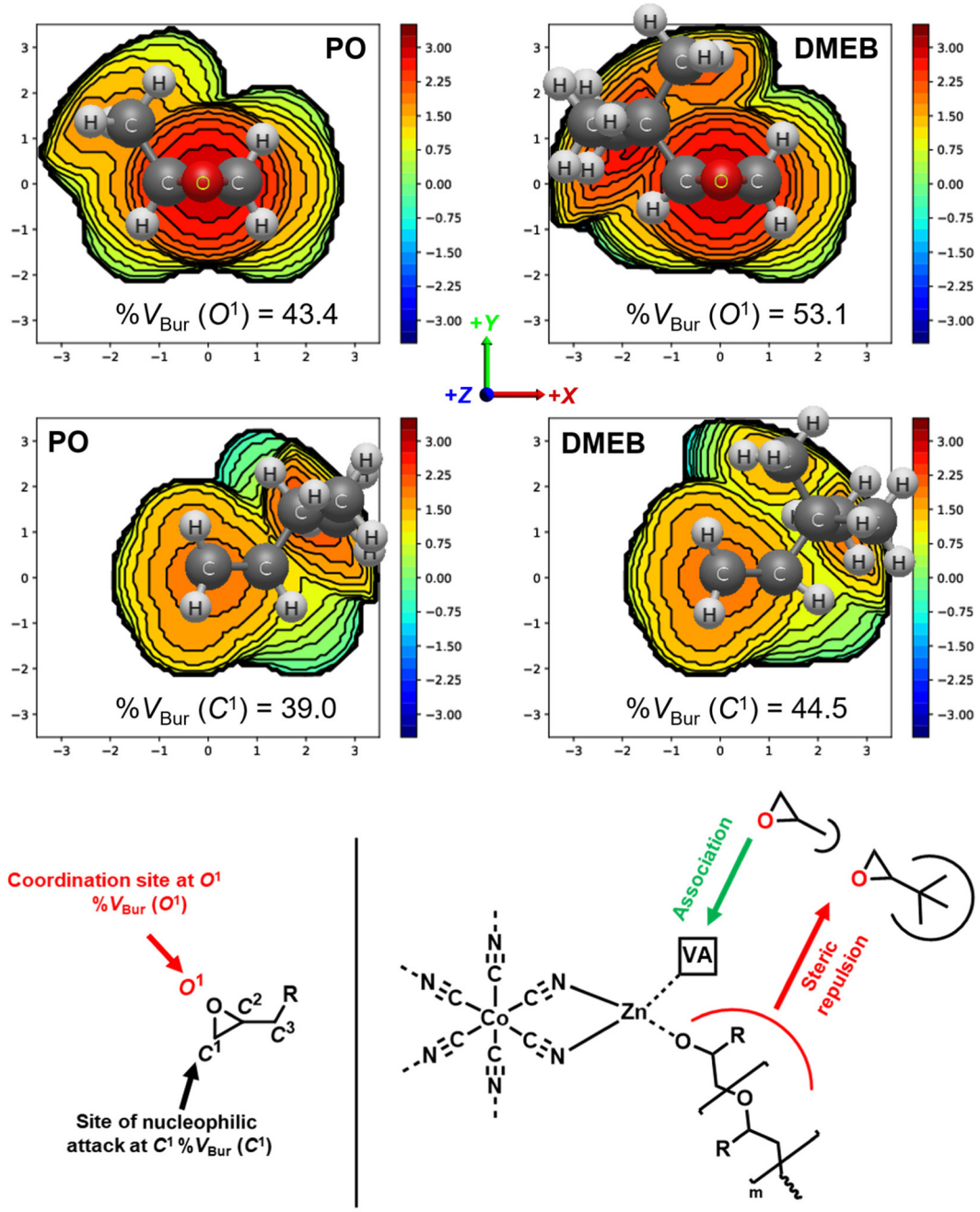

Fig. 4 Top: steric maps of PO and DMEB for the oxygen of the epoxide ring O^1 and the unsubstituted methylene carbon C^1 in the direction of the *Z*-axis. Bottom left: schematic representation of the coordination site and the site of nucleophilic attack. Bottom right: proposed inhibition of DMEB polymerization *via* DMC catalysis due to steric repulsion.

mers (Table 3). Notably, GME exhibits a significantly larger ΔN than PO and EO (ΔN_{GME} = 0.090, ΔN_{EO} = 0.078 > ΔN_{PO} = 0.077), which implies a potentially favored coordination of GME at the catalyst's Zn^{2+} active site compared to other monomers.[12] In addition, all glycidyl ethers contain a second oxygen (O^2) bearing a negative partial charge (SI, Table S6) comparable to the epoxide oxygen O^1. Therefore, the ether oxygen O^2 could further act as an auxiliary donor and enable bidentate binding to the Zn site (Scheme 2), further strengthening the monomer–catalyst association, like a mechanism previously described for glycidol.[26] As the steric demand of R^1 increases, the ability of O^2 to coordinate Zn decreases. This is further accompanied by a reduction in the partial charge at O^2 for the phenyl-glycidyl ether derivatives PGE and MPGE, explaining the observed low reactivity of both monomers. In this regard, the monomer structure of GME is a near-perfect match, combining the least steric demand among all GE monomers with the highest predicted affinity to the catalyst due to its elec-

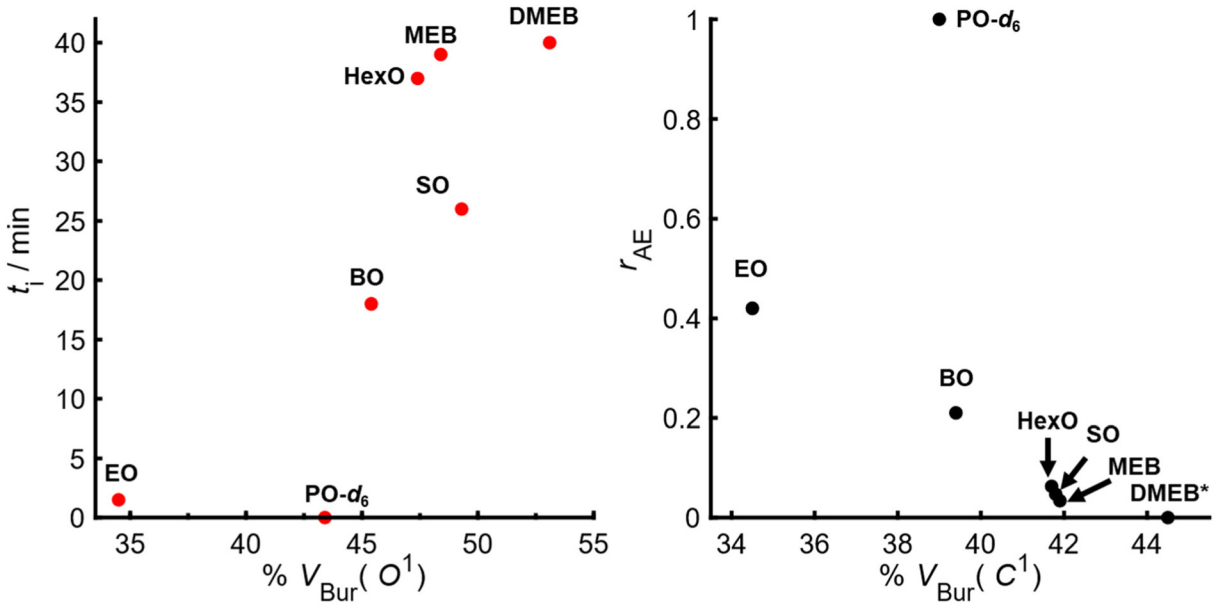

Fig. 5 Left: determined induction times for the experiment with the respective comonomer plotted *vs.* %$V_{Bur}(O^1)$ of the respective comonomer. Right: determined reactivity ratios of comonomers plotted *vs.* %$V_{Bur}(C^1)$ of the respective comonomer. *DMEB was included as a reference point with r_{DMEB} set to 0.

Table 3 Reactivity ratios, induction times and half-lives determined for the copolymerization of PO with glycidyl ether (GE) comonomers *via* the integrated ideal model

Comonomer	Structure	r_{PO}	r_{Co}	t_i/min	$t_{1/2}$ (PO)/min	$t_{1/2}$ (Co)/min	ΔN
GME[Bulk a]	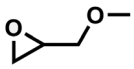	1.40	0.71		~12	~17	0.090
AGE	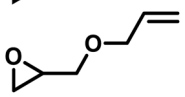	9.2	0.11	8	1.5	13	0.052
BGE	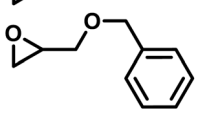	12	0.081	75	12	140	0.047
FGE	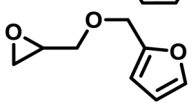	14	0.073	104	18	269	0.071
PGE	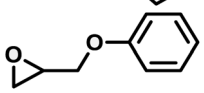	14	0.073	235	12	157	0.072
MPGE	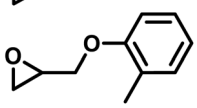	17	0.060	116	8.7	137	0.083

[a] Values previously reported by Matthes *et al. via* the Jaacks fit for the copolymerization kinetic experiment in bulk at 80 °C; no induction period could be observed.[29]

tronic structure. Similar to PO and to the trend observed for AlkO and ArO monomers (Table 2), even slight deviations of the GE monomer structure from GME led to a marked reduction in monomer reactivity.

All glycidyl ethers except GME and AGE show a drastic increase in induction times and half-lives of both PO and GE comonomers (Table 3). These findings further support the proposed monomer-adsorption mechanism (Scheme 2). Here, the propagation of the polymerization can only commence *via* mode (A3), as shown in Scheme 3, while potential coordination modes (A1) and (A2) result in the experimentally observed inhibitive effect of glycidyl ethers on DMC catalysis.

Furthermore, the corresponding SEC traces of all copolymerization experiments of PO with glycidyl ethers are shown

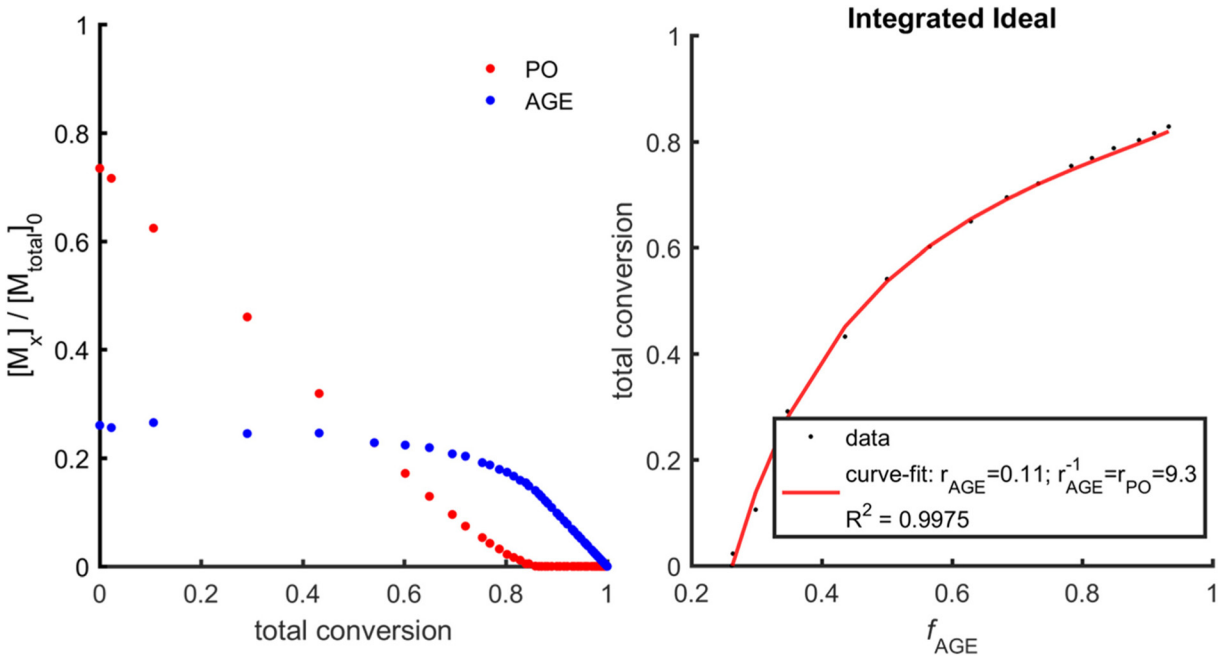

Fig. 6 DMC-catalyzed copolymerization of PO (red) and AGE (blue). Left: individual monomer concentrations [M_x] normalized by the total monomer concentration $[M_{total}]_0$ plotted *vs.* the total conversion of both monomers for the time interval of copolymerization after the induction period. Right: ideal integrated fit for the determination of reactivity ratios.

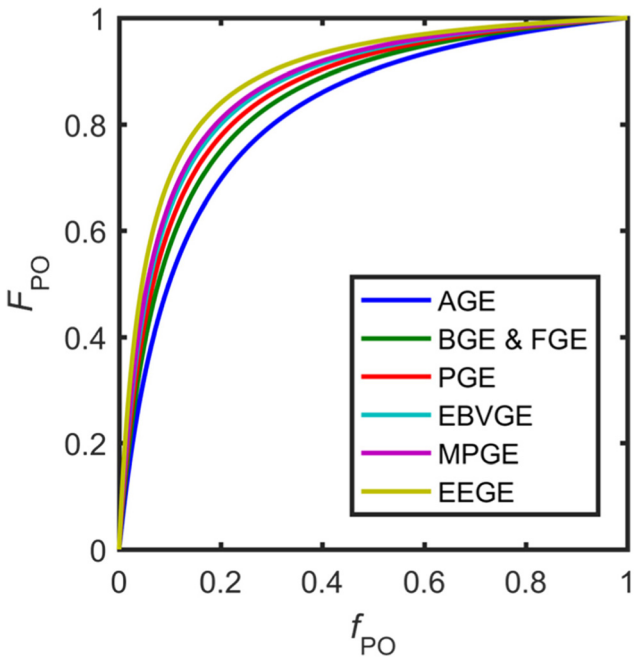

Fig. 7 Copolymerization diagrams for DMC-catalyzed copolymerizations of PO with glycidyl ethers (GE).

in Fig. S18 (SI). Compared to the copolymerization experiments of the alkyl and aryl epoxides, the molecular weight distributions of GE-based copolymers showed a significantly higher molecular weight tailing and considerably broader dispersities ranging from $Đ$ = 1.18 to 2.17. Here, we observed an overall trend in which the comonomers associated with prolonged induction times yielded copolymers with markedly higher dispersities. For instance, the resulting copolymers P(PO-*co*-MPGE) ($Đ$ = 1.56), P(PO-*co*-FGE) ($Đ$ = 2.17) and P(PO-*co*-FGE) ($Đ$ = 1.99) showed the broadest molecular weight distributions in this study and also exhibited the longest induction periods, with t_i (FGE) = 104 min, t_i (MPGE) = 116 min and t_i (PGE) = 235 min (Table 3). This correlation between a decrease in catalyst activity, prolonged induction time, and an increase in dispersity, as well as higher molecular weight tailing of the resulting polymer, has also been reported in other works on DMC-catalyzed propoxylation reactions.[14,15,17,45] We propose that unreactive comonomers like FGE and PGE may further act as blocking agents, inhibiting PO coordination at the catalyst surface and catalyst activation and significantly reducing the effect of "catch-up" kinetics during the copolymerization. In contrast, the P(PO-*co*-AGE) copolymer shows a similarly broad molecular weight distribution ($Đ$ = 1.61) despite a comparatively short induction period (t_i (AGE) = 8 min). Since this copolymer contains reactive double bonds, a certain extent of crosslinking during or after the copolymerization experiment may account for the higher molecular weight tailing and the bimodality observed in the SEC trace, thereby explaining the deviation from the trend described above (SI, Fig. S18).

Copolymerization of PO with glycidyl ether acetals and glycidyl esters

As the synergy of electronic structure and sterics is crucial for the monomer reactivity of glycidyl ethers in DMC catalysis, we

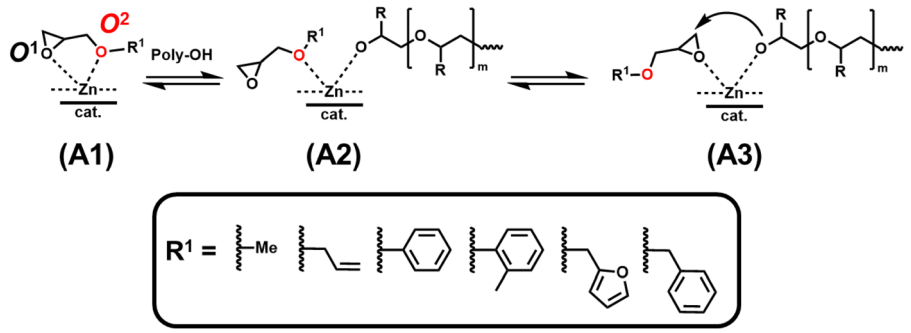

Scheme 2 Proposed coordination modes of glycidyl ethers (GE) at the active Zn site of the DMC catalyst.

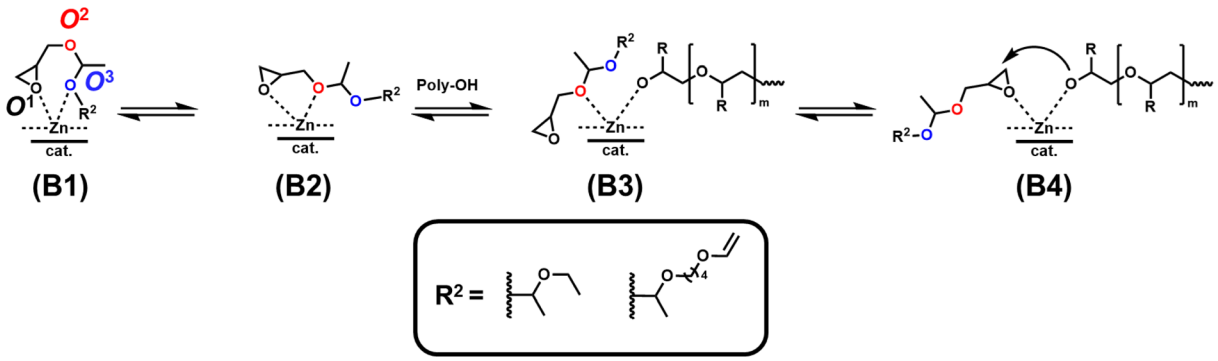

Scheme 3 Proposed coordination modes of EEGE and EBVGE at the active Zn site of the DMC catalyst.

expanded our kinetic investigations to epoxide monomers with multiple oxygen atoms in the substituent side chain, namely the glycidyl ether acetals and glycidyl esters presented in Table 4. The first monomer of this class we investigated was ethoxy ethyl glycidyl ether (EEGE), as this comonomer is commonly employed for tailoring the thermoresponsiveness of polyether copolymers and the synthesis of linear polyglycerol.[46] The copolymerization of PO and EEGE has already been investigated for the conventional AROP by Schömer *et al.*[47] Reinvestigation of the ^{1}H NMR kinetic data from this

Table 4 Reactivity ratios, induction times and half-lives determined for the copolymerization of PO with glycidyl ether acetal and glycidyl ester (GEs) comonomers *via* the integrated ideal model

Comonomer	Structure	r_{PO}	r_{Co}	t_i/min	$t_{1/2}$ (PO)/min	$t_{1/2}$ (Co)/min	ΔN
EBVGE	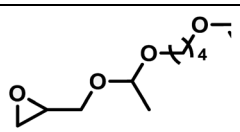	16	0.064	29	4.0	55	0.087
EEGE[Bulk a]	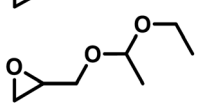	21	0.048	76	9.3	223	0.075
GMA	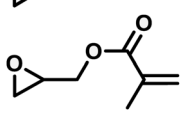	20	0.050	40	9.2	179	0.000
GBz	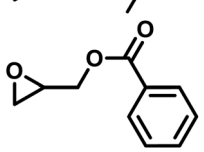	33	0.031	77	14	452	0.003

[a] Copolymerization kinetic experiment conducted in bulk at 80 °C.

work with the fits of the integrated ideal model revealed the reactivity ratios r_{PO} = 0.23 and r_{EEGE} = 4.4 (SI, Fig. S13).

These reactivity ratios indicate the formation of a gradient structure constituted by a predominant incorporation of EEGE units at the beginning of the polymer chains and PO units at the end. Gervais and coworkers investigated the same system under conditions of the monomer-activated AROP (MAROP) and determined reactivity ratios of r_{PO} = 3.58 and r_{EEGE} = 0.18.[48] This corresponds to an inversion of the reactivity compared to the classical AROP and leads to predominant incorporation of PO units at the beginning of the polymer chains and EEGE-rich domains at the end. In the current work, this comonomer system was investigated under DMC catalysis in bulk for better comparison with previously reported kinetic data for the PO/GME pair.[29] Interestingly, the induction period of the copolymerization of PO/EEGE, 76 min, greatly exceeds the observed t_i of other short-chain GE monomers such as GME and AGE (Table 3) and is thus more comparable to BGE. As shown in Fig. 8, PO was consumed significantly faster compared to EEGE. The monomer concentration of EEGE hardly changed in the presence of PO and only decreased after full conversion of PO. This is further reflected in the reactivity ratios of r_{PO} = 21 and r_{EEGE} = 0.048 (Fig. 8), which follow the same trend and preference for PO polymerization as in MAROP. However, under the conditions of DMC catalysis, this divergence in comonomer reactivity is significantly more pronounced, indicating the formation of P(PO-*co*-EEGE) with a potentially near-tapered block copolymer structure. The copolymerization behavior of this monomer pair proved to be highly dependent on the copolymerization method. The different conditions of AROP, MAROP and DMC catalysis cause extreme changes in the reactivity ratios of this comonomer pair. A similar behavior was reported by our group for the copolymerization of EO and PO.[28]

We further investigated the copolymerization of PO with the bulky glycidyl ether acetal derivative ethoxy butoxy vinyl glycidyl ether (EBVGE). Our group recently developed EBVGE to introduce acid-cleavable acetal and reactive vinyl groups into the poly(ethylene glycol) (PEG) backbone, thereby combining the functionalities of AGE and EEGE.[49] From the fits shown in Fig. S12 (SI), the reactivity ratios r_{PO} = 16 and r_{EBVGE} = 0.064 were obtained. In contrast to the previously observed decrease in monomer reactivity for the bulky AlkO/ArO and GE monomers, here, the sterically demanding EBVGE demonstrates a significantly higher monomer reactivity and shorter t_i and $t_{1/2}$ compared to EEGE. Due to the increased ΔN, the monomer–catalyst coordination affinity is expected to be higher compared to EEGE, but furthermore, the sterically demanding R^2 group can potentially inhibit coordination modes of the monomer *via* oxygen O^3, as presented in Scheme 3 (B1).

As for EEGE, the inactive coordination modes (B1), (B2) and (B3) *via* coordination of the electron negative oxygens O^2 and O^3 (SI, Table S6) might result in catalyst deactivation and therefore explain the experimentally observed high monomer half-life of 223 min (Table 4).

The last group of the investigated comonomers comprised two glycidyl esters. Glycidyl methacrylate (GMA) is of considerable interest due to its orthogonal double bond, which can be radically polymerized or modified by thiol–ene click chemistry.

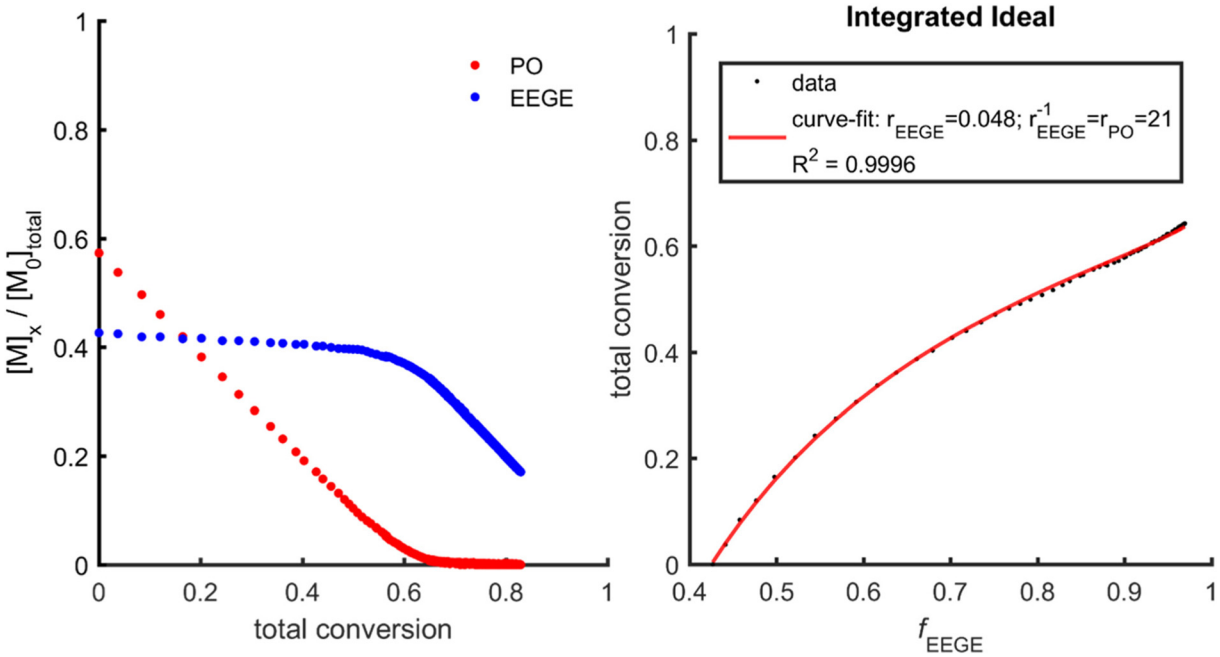

Fig. 8 DMC-catalyzed copolymerization of PO (red) and EEGE (blue). Left: individual monomer concentrations [M_x] normalized by the total monomer concentration $[M_{total}]_0$ plotted *vs.* the total conversion of both monomers for the time interval of copolymerization after the induction period. Right: ideal integrated fit for the determination of reactivity ratios.

The reactivity ratios were similar to those of EEGE, with r_{PO} = 20 and r_{GMA} = 0.050 (SI, Fig. S16). Due to the highly reactive methacrylate moieties, crosslinking side reactions were observed during later stages of the copolymerization. Consequently, no SEC trace of this copolymer is available in this study. Controlled bulk copolymerization of PO and GMA under DMC catalysis under optimized reaction conditions, including comparable reactivity ratios for this comonomer pair, will be reported in a separate study. Another representative glycidyl ester is glycidyl benzoate (GBz), which was next to the unreactive DMEB, the least reactive comonomer in the copolymerization kinetic studies with PO. The comonomer pair PO/GBz showed extremely divergent reactivity ratios of r_{PO} = 33 and r_{GBz} = 0.031 (Table 4 and SI, Fig. S17). The SEC trace of the PO/GBz copolymer is shown in Fig. S18 (SI) and exhibits low dispersity of $Đ$ = 1.22. The copolymerization diagram for PO with glycidyl esters is shown in Fig. 9 and implies the formation of a tapered block copolymer.

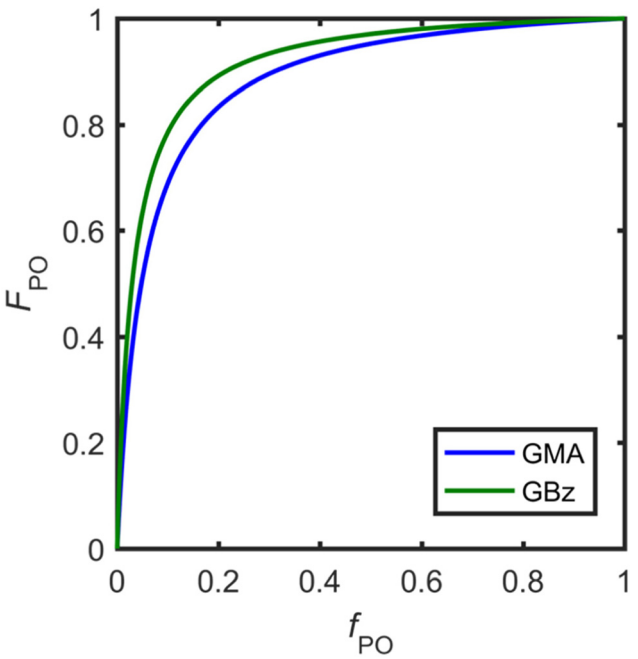

Fig. 9 Copolymerization diagrams for DMC-catalyzed copolymerizations of PO with glycidyl esters (GEs).

DFT calculations revealed low ΔN values for both monomers (Table 4) compared to PO (Table 2), suggesting a weak coordination tendency of glycidyl ester comonomers toward the Zn site of the catalyst. Additionally, O^3 carries a more negative Hirshfeld charge than O^1 and O^2, suggesting preferential coordination *via* the carbonyl oxygen at the Zn site (Scheme 4; (C3)). These computations support the experimentally observed low monomer reactivity of glycidyl esters and explain the very long half-lives of up to 452 min for this class of monomers (Table 4).

Summarizing the findings of our kinetic study, we identified steric effects as the primary determinant of monomer reactivity for alkylene oxides and aryl epoxides in the DMC catalyst. For glycidyl ethers, the change in electronic structure imposed by the adjacent ether motif significantly influences the monomer behavior in DMC catalysis. When the number of oxygen atoms in the side chain is further increased, as in glycidyl ether acetals and glycidyl esters, the electronic structure of the monomer becomes the dominant factor governing monomer reactivity, with additional coordination of the comonomer side chain potentially explaining the observed inhibition of catalyst activation.

Conclusion

DMC catalysis for the synthesis of PPO and PPO-based polyol star polymers (polyether polyols) is highly established due to the resulting narrow molecular weight distributions and low level of side reactions. In this study, the application of DMC catalysis for the copolymerization of PO with a variety of epoxide comonomers has been investigated. The heterogeneous, coordinative DMC-catalyzed copolymerizations were monitored by *in situ* ^{1}H NMR spectroscopy, revealing surprising differences in reactivity, with PO being always the more reactive monomer. The pendant group at the oxirane ring has a dramatic influence on the reactivity of the monomers in the coordinative copolymerization. The bulkier the substituent, the lower is the observed reactivity of the epoxide. In particu-

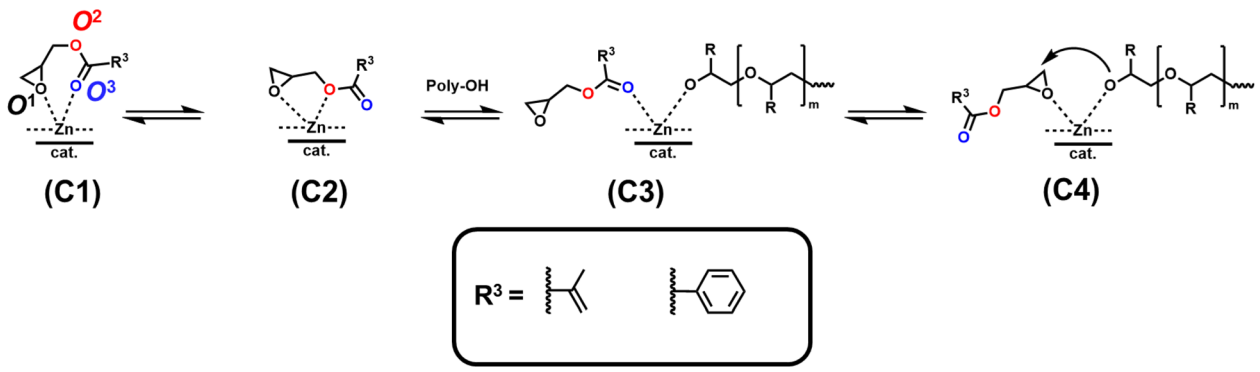

Scheme 4 Proposed coordination modes of glycidyl esters (GEs) at the active Zn site of the DMC catalyst.

lar, the steric demand of the α-carbon for alkylene oxides plays a crucial role in the observed trends, since even slight deviations from the PO geometry led to a drastic decrease in monomer reactivity and a slight increase in induction times. Besides DMEB, all epoxide monomers presented in this study proved to be highly compatible with the DMC catalyst. Glycidyl ethers and esters led to partial deactivation of the DMC catalyst, resulting in prolonged induction times and overall lower reaction rates. For this class of epoxide monomers, electronic effects appeared to be as important as the geometry of the monomer. In this regard, GME is the ideal glycidyl ether structure, combining a strong tendency towards coordination at the active Zn site of the catalyst, expressed by a high fraction of electron transfer (ΔN), while still maintaining the low steric demand and a comparable geometry to PO. We hesitate to directly translate the observed reactivity ratios to gradients in the polymer structure, since the mechanism of the DMC-catalyzed copolymerization shows peculiarities, such as the catch-up effect, in stark contrast to living copolymerizations that are characterized by the absence of termination and chain transfer. However, the observed reactivity ratios may imply the formation of gradient and, in some cases, tapered block-like microstructures. Throughout all experiments, the DMC catalyst demonstrated an exceptionally high substrate specificity for PO in comparison with other epoxide monomers. DMC catalysis has been proven to be a very effective and powerful technique for the copolymerization of PO with various epoxide comonomers. These results are valuable for the synthesis of multifunctional PPO and the design of new gradient and tapered block-like copolymers with special properties.

Conflicts of interest

The authors declare no competing financial interest.

Data availability

The data supporting this article have been included as part of the supplementary information (SI). Supplementary information: Instrumentation, detailed experimental and synthetic procedures for EEGE, EVGE and GBz, evaluation of *in situ* ^{1}H NMR copolymerization kinetic experiments, copolymer characterization data (SEC and MALDI-ToF MS), DFT calculations, Hirshfeld atomic charges, values for buried volumes, Cartesian coordinates for optimized geometries. See DOI: https://doi.org/10.1039/d6py00118a.

Acknowledgements

The authors thank BASF SE for financial support and for providing the DMC catalyst. J. B. thanks the Graduate School "Materials Science in Mainz (MAINZ)" for financial support. M. K. thanks the Max Planck Graduate Center for financial support. The authors like to thank Rebecca Matthes, Andreas Haedler and Ruth Lohwasser for valuable discussions and conceptualization of this work.

References

1 A. de Lucas, L. Rodríguez, M. Pérez-Collado, P. Sánchez and J. F. Rodríguez, *Polym. Int.*, 2002, **51**, 1066–1071.
2 (*a*) D. M. Simons and J. J. Verbanc, *J. Polym. Sci.*, 1960, **44**, 303–311; (*b*) G.-E. Yu, F. Heatley, C. Booth and T. G. Blease, *J. Polym. Sci., Part A: Polym. Chem.*, 1994, **32**, 1131–1135.
3 M. Ionescu, *Chemistry and technology of polyols for polyurethanes*, Rapra Technology, Shawbury, Shrewsbury, Shropshire, UK, 2005.
4 J. Milgrom, *US Pat*, 3278457, 1963.
5 R. A. Livigni, R. J. Herold, O. C. Elmer and S. L. Aggarwal, *ACS Symp. Ser.*, 1975, **6**, 20–37.
6 J. M. O'Connor, D. L. Lickei and R. L. Grieve, *US Pat*, 6359101, 1999.
7 H. van der Hulst, G. A. Pogany and J. Kuyper, *US Pat*, 4477589, 1982.
8 I. Kim, J.-T. Ahn, C. S. Ha, C. S. Yang and I. Park, *Polymer*, 2003, **44**, 3417–3428.
9 Y.-J. Huang, G.-R. Qi and Y.-H. Wang, *J. Polym. Sci., Part A: Polym. Chem.*, 2002, **40**, 1142–1150.
10 J. Hofmann, P. Ooms, P. Gupta and W. Schäfer, *US Pat*, US6291388B1, 2000.
11 L.-C. Wu, A.-F. Yu, M. Zhang, B.-H. Liu and L.-B. Chen, *J. Appl. Polym. Sci.*, 2004, **92**, 1302–1309.
12 C. H. Tran, H. B. Jang, B. Moon, E. Lee, H. Choi and I. Kim, *Catal. Today*, 2024, **425**, 114319.
13 K. G. McDaniel, *US Pat*, US2008167501A1, 2007.
14 R. Bachmann, M. Klinger and A. Jupke, *Macromol. Theory Simul.*, 2021, **30**, 2100012.
15 M. Klinger, R. Bachmann and A. Jupke, *Macromol. Theory Simul.*, 2021, **30**, 2100013.
16 Y.-J. Huang, X.-H. Zhang, Z.-J. Hua, S.-L. Chen and G.-R. Qi, *Macromol. Chem. Phys.*, 2010, **211**, 1229–1237.
17 S.-F. Stahl and G. A. Luinstra, *React. Chem. Eng.*, 2024, **9**, 91–107.
18 I. E. Nifant'ev and P. V. Ivchenko, *Int. J. Mol. Sci.*, 2024, **25**, 10695.
19 J. Herzberger, K. Niederer, H. Pohlit, J. Seiwert, M. Worm, F. R. Wurm and H. Frey, *Chem. Rev.*, 2016, **116**, 2170–2243.
20 (*a*) Y. J. Huang, G. R. Qi and L. S. Chen, *Appl. Catal., A*, 2003, **240**, 263–271; (*b*) X.-H. Zhang, Z.-J. Hua, S. Chen, F. Liu, X.-K. Sun and G.-R. Qi, *Appl. Catal., A*, 2007, **325**, 91–98; (*c*) S. Chen, P. Zhang and L. Chen, *Prog. Org. Coat.*, 2004, **50**, 269–272; (*d*) C. H. Tran, L. T. T. Pham, H. B. Jang, S. A. Kim and I. Kim, *Catal. Today*, 2021, **375**, 429–440; (*e*) C.-H. Tran, M.-W. Lee, S.-J. Lee, J.-H. Choi, E. Lee, H. Choi and I. Kim, *Polymers*, 2022, **14**, 2507; (*f*) I. K. Lee, J. Y. Ha, C. Cao, D.-W. Park, C.-S. Ha and I. Kim, *Catal. Today*, 2009, **148**, 389–397.
21 (*a*) G. P. Johari, A. Hallbrucker and E. Mayer, *J. Polym. Sci., Part B: Polym. Phys.*, 1988, **26**, 1923–1930; (*b*) K. L. Peretti,

H. Ajiro, C. T. Cohen, E. B. Lobkovsky and G. W. Coates, *J. Am. Chem. Soc.*, 2005, **127**, 11566–11567.

22 (*a*) Y. Deng, J. Ding, G. Yu, R. H. Mobbs, F. Heatley, C. Price and C. Booth, *Polymer*, 1992, **33**, 1959–1962; (*b*) H.-W. Engels, H.-G. Pirkl, R. Albers, R. W. Albach, J. Krause, A. Hoffmann, H. Casselmann and J. Dormish, *Angew. Chem., Int. Ed.*, 2013, **52**, 9422–9441; (*c*) X. Paredes, A. S. Pensado, M. J. P. Comuñas and J. Fernández, *J. Chem. Eng. Data*, 2010, **55**, 4088–4094.

23 H. N. Hampson and E. R. A. Forshaw, *US Pat*, 3336242A, 1961.

24 X. Hong, J. Zhao and G. Zhang, *Macromol. Rapid Commun.*, 2025, e00684.

25 (*a*) R.-J. Wei, X.-H. Zhang, Y.-Y. Zhang, B.-Y. Du, Z.-Q. Fan and G.-R. Qi, *RSC Adv.*, 2014, **4**, 3188–3194; (*b*) R.-J. Wei, Y.-Y. Zhang, X.-H. Zhang, B.-Y. Du and Z.-Q. Fan, *RSC Adv.*, 2014, **4**, 21765–21771.

26 C. H. Tran, M. W. Lee, S. A. Kim, H. B. Jang and I. Kim, *Macromolecules*, 2020, **53**, 2051–2060.

27 (*a*) L. Hu, X. Zhang, X. Cao, D. Chen, Y. Sun, C. Zhang and X. Zhang, *Macromolecules*, 2021, **54**, 6182–6190; (*b*) X.-H. Zhang, R.-J. Wei, Y. Zhang, B.-Y. Du and Z.-Q. Fan, *Macromolecules*, 2015, **48**, 536–544; (*c*) W. S. Jae, H. Choi, H. S. Lee, C. H. Tran, C. H. Le Tran, K. A. Trinh and I. Kim, *Polymers*, 2025, **17**, 2458.

28 J. Blankenburg, E. Kersten, K. Maciol, M. Wagner, S. Zarbakhsh and H. Frey, *Polym. Chem.*, 2019, **10**, 2863–2871.

29 R. Matthes, C. Bapp, M. Wagner, S. Zarbakhsh and H. Frey, *Macromolecules*, 2021, **54**, 11228–11237.

30 (*a*) M. Hesse, G. M. Linden and H. Frey, *Macromolecules*, 2025, **58**, 13300–13313; (*b*) V. Rejsek, D. Sauvanier, C. Billouard, P. Desbois, A. Deffieux and S. Carlotti, *Macromolecules*, 2007, **40**, 6510–6514.

31 F. T. Wall, *J. Am. Chem. Soc.*, 1941, **63**, 1862–1866.

32 V. Jaacks, *Makromol. Chem.*, 1972, **161**, 161–172.

33 B. S. Beckingham, G. E. Sanoja and N. A. Lynd, *Macromolecules*, 2015, **48**, 6922–6930.

34 J. Blankenburg, M. Wagner and H. Frey, *Macromolecules*, 2017, **50**, 8885–8893.

35 J. Qiu, B. Charleux and K. Matyjaszewski, *Prog. Polym. Sci.*, 2001, **26**, 2083–2134.

36 J. Blankenburg, M. Wagner and H. Frey, *Macromolecules*, 2017, **50**, 8885–8893.

37 C.-H. Tran, M.-W. Lee, S.-W. Park, J.-E. Jeong, S.-J. Lee, W. Song, P. Huh and I. Kim, *Catalysts*, 2021, **11**, 1033.

38 (*a*) L. Falivene, R. Credendino, A. Poater, A. Petta, L. Serra, R. Oliva, V. Scarano and L. Cavallo, *Organometallics*, 2016, **35**, 2286–2293; (*b*) L. Falivene, Z. Cao, A. Petta, L. Serra, A. Poater, R. Oliva, V. Scarano and L. Cavallo, *Nat. Chem.*, 2019, **11**, 872–879.

39 S. Escayola, N. Bahri-Laleh and A. Poater, *Chem. Soc. Rev.*, 2024, **53**, 853–882.

40 (*a*) M. Magre, E. Paffenholz, B. Maity, L. Cavallo and M. Rueping, *J. Am. Chem. Soc.*, 2020, **142**, 14286–14294; (*b*) F. Butler, F. Fiorentini, K. H. S. Eisenhardt and C. K. Williams, *Macromolecules*, 2025, **58**, 7150–7160.

41 C. H. Tran, L. T. T. Pham, Y. Lee, H. B. Jang, S. Kim and I. Kim, *J. Catal.*, 2019, **372**, 86–102.

42 R. Mohr, M. Wagner, S. Zarbakhsh and H. Frey, *Macromol. Rapid Commun.*, 2021, **42**, e2000542.

43 B. F. Lee, M. J. Kade, J. A. Chute, N. Gupta, L. M. Campos, G. H. Fredrickson, E. J. Kramer, N. A. Lynd and C. J. Hawker, *J. Polym. Sci., Part A: Polym. Chem.*, 2011, **49**, 4498–4504.

44 M. J. Barthel, T. Rudolph, A. Teichler, R. M. Paulus, J. Vitz, S. Hoeppener, M. D. Hager, F. H. Schacher and U. S. Schubert, *Adv. Funct. Mater.*, 2013, **23**, 4921–4932.

45 S. Lee, S. T. Baek, K. Anas, C.-S. Ha, D.-W. Park, J. W. Lee and I. Kim, *Polymer*, 2007, **48**, 4361–4367.

46 (*a*) V. Müller, R. Matthes, M. Wagner, M. Bros, P. Dreier and H. Frey, *Polym. Chem.*, 2023, **14**, 2599–2609; (*b*) R. K. Kainthan, J. Janzen, E. Levin, D. V. Devine and D. E. Brooks, *Biomacromolecules*, 2006, **7**, 703–709; (*c*) A. Thomas, S. S. Müller and H. Frey, *Biomacromolecules*, 2014, **15**, 1935–1954.

47 M. Schömer and H. Frey, *Macromolecules*, 2012, **45**, 3039–3046.

48 M. Gervais, A.-L. Brocas, G. Cendejas, A. Deffieux and S. Carlotti, *Macromolecules*, 2010, **43**, 1778–1784.

49 K. Maciol, Ph. D. Dissertation, Johannes Gutenberg-University Mainz, 2018.